

Dimerized Decomposition of Quantum Evolution on an Arbitrary Graph

He Feng,^{1,2} Tian-Min Yan,^{1,*} and Y. H. Jiang^{1,2,3,†}

¹Shanghai Advanced Research Institute, Chinese Academy of Sciences, Shanghai 201210, China

²University of Chinese Academy of Sciences, Beijing 100049, China

³ShanghaiTech University, Shanghai 201210, China

The study of quantum evolution on graphs for diversified topologies is beneficial to modeling various realistic systems. A systematic method, the dimerized decomposition, is proposed to analyze the dynamics on an arbitrary network. By introducing global "flows" among interlinked dimerized subsystems, each of which locally consists of an input and an output port, the method provides an intuitive picture that the local properties of the subsystem are separated from the global structure of the network. The pictorial interpretation of quantum evolution as multiple flows through the graph allows for the analysis of the complex network dynamics supplementary to the conventional spectral method.

PACS numbers: 02.50.-r, 02.10.Yn, 89.75.Hc

I. INTRODUCTION

The quantum evolution on a network, which consists of multiple sites and edges representing inter-site couplings, appeals increasing interests for its wide applications ranging from quantum information [1] and computation [2] to excitation transfer [3]. Typically, the quantity of interest is the transport efficiency or the transfer time to specific site(s), e.g., the maximized probability at the target site in the shortest time for the spatial search algorithm [4], the enhanced efficiency of energy transfer assisted by coherence among chromophores in photosynthetic complexes [5], and the maximum fidelity to transmit a quantum state in a spin-network from one point to another [6]. In general, the processes can be rephrased within the theoretical framework of continuous-time quantum walk (CTQW) [7], which outperforms the classical counterpart by exploiting interference among different paths in a graph. The experimental implementations of CTQW are proposed or achieved on various platforms including ultracold Rydberg atoms [8, 9], tight-binding graphene lattice [10, 11], and optical waveguide lattices [12–14].

Within the framework of CTQW, the techniques of dimensionality reduction that project the complete space spanned by sites of the original system to an equivalent one, or a subspace, have usually been applied, e.g., the invariant subspace methods using the Lanczos algorithm for systems of proper symmetry [15], diagrammatic approach by degenerate perturbation theory [16–18]. These methods considerably reduce the complexity and provide simplified pictures analogous to well-known problems, e.g., the linear chain decomposition that transforms a dendrimer to a line [19] or linear chains [20], and transport equivalent quantum networks mapping onto classical resistor networks [21].

In this work, a reduction scheme, the dimerized decomposition, is introduced to simplify the analysis of quantum

evolution on graphs. The approach diverts our attention from the amplitudes on sites towards *flows*, the relations among sites, within the graph. Given an N -site graph with M coupling edges, the method serves to decompose the graph into M subsystems, each of which includes only two sites. Within the subsystem, the dynamics are governed by the equation of motion (EOM) similar to an ordinary Schrödinger equation with its local Hamiltonian containing the information of site energies, local coupling, and explicit numbers of connectivities. The two sites within the subsystem form a pair of ports, via which the local subsystem is connected to other subsystems through auxiliary boundary terms, interpreted as inter-subsystem "flows". Once the relations of amplitudes among subsystems are set, the flows are determined. More specifically, the relations yield a series of matching conditions in the form of a linear system encoded by the global topologies, and the flows are obtained by solving the linear system. The method provides an intuitive picture that may simplify the design or optimization of desired quantities, e.g., the efficiency of quantum transport.

The work is organized as follows: in Sec. II, we introduce the dimerized decomposition and the EOM of the subsystem after the decomposition. The validity of the method is shown starting with Schrödinger equation for the quantum evolution on a generic graph. In Sec. III, two examples using the decomposition are presented. The explicit expression of the EOMs of subsystems are shown in Sec. III A with the matching conditions given in III B for a diamond graph, then in Sec. III B the transport efficiency of a trimer system is analyzed using the method.

II. THEORY OF DIMERIZED DECOMPOSITION

Given an undirected graph $G = (V, E)$ consisting of the vertex set V and edge set E , we start by decomposing the full system into subsystems $\{\mathcal{S}\}$, each of which is

* yantm@sari.ac.cn

† jiangyh@sari.ac.cn

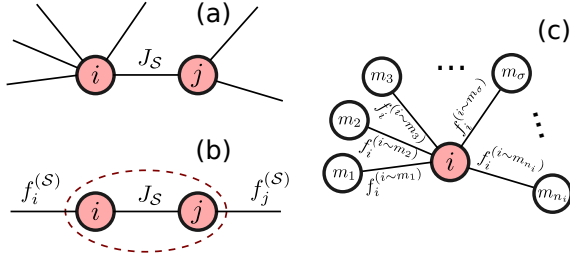


Figure 1. The scheme of dimerized decomposition in a graph. An arbitrary pair of sites i and j that are coupled by edge of J_S , as shown by (a), can be viewed to form a local subsystem (b), which is effectively isolated from the global network structure if all effects of inter-subsystem communication are solely described by flows of two ports, the auxiliary functions $f_i^{(S)}$ and $f_j^{(S)}$. Figure (c) shows how the EOM of the subsystem formed by any pair of coupled sites i and m_σ is derived. Assuming an arbitrary site i in the graph is connected to n_i neighboring sites, for each connection between site i and m_σ there introduced an auxiliary function $f_i^{(i\sim m_\sigma)}$.

associated with a local Hamiltonian $\hat{H}^{(S)}$. The dimerized decomposition gains its name from the scheme that each subsystem is constructed from the pair of coupled sites, namely, the edge $\mathcal{S} = (i \sim j) \in E$. In general, the subsystems are allowed to communicate with each other and the mechanism can be realized via inter-subsystem flows. With the above setup, it is shown that the original full Schrödinger equation for the quantum evolution on the graph can be casted into a set of coupled EOMs of subsystems $\{\mathcal{S}\}$.

As shown in Fig. 1(a), we consider the coupled sites i and j with energies ε_i and ε_j , respectively. The coupling strength of the associated edge is J_S . Sites i and j together with edge \mathcal{S} form the primitive subsystem \mathcal{S} as shown in Fig. 1(b). Besides the intra-subsystem coupling J_S , the two sites may also be connected to sites outside \mathcal{S} . These multiple connections except for J_S may be simplified by an equivalent term, defined in our work as the time-dependent flow function $f_i^{(S)}(t)$. As appeared in Fig. 1(b), flows $f_i^{(S)}(t)$ and $f_j^{(S)}(t)$ are introduced for sites i and j , respectively. In the following we show the validity of such decomposition and derive the EOM within the subsystem in terms of flows.

Without loss of generality, we start the decomposition from a single arbitrary site i as shown in Fig. 1. Let $c_i(t)$ be the amplitude of site i in the full system (i.e., before the decomposition). With the total number of connections of site i defined by connectivity n_i , all edges coupled to i form a set $\mathcal{S}_i = \{i \sim m_\sigma | \sigma = 1, \dots, n_i\}$. From Schrödinger equation, the EOM for site i reads

$$\dot{c}_i(t) = -i\varepsilon_i c_i(t) - i \sum_{\sigma=1}^{n_i} J_{i\sim m_\sigma} c_{m_\sigma}(t), \quad (1)$$

where $i \sim m_\sigma$ denotes site i is connected to site m_σ . For brevity, time variable t (and variable s in the Laplace s -domain as will be introduced later) is henceforth dropped

from functions, unless noted otherwise.

Let $c_i = \sum_{\mathcal{S} \in \mathcal{S}_i} c_i^{(S)}$ and substitute the sum into Eq. (1),

$$\sum_{\mathcal{S} \in \mathcal{S}_i} \dot{c}_i^{(S)} = -i\varepsilon_i \sum_{\mathcal{S} \in \mathcal{S}_i} c_i^{(S)} - i \sum_{\sigma=1}^{n_i} J_{i\sim m_\sigma} \sum_{\mathcal{S} \in \mathcal{S}_{m_\sigma}} c_{m_\sigma}^{(S)} \quad (2)$$

With the aim to separate the component $c_i^{(S)} = c_i^{(i\sim m_1)}$ from the sum, we introduce an auxiliary function $f_i^{(i\sim m_1)}$ and Eq. (2) is split as followings,

$$\begin{aligned} \dot{c}_i^{(i\sim m_1)} &= -i\varepsilon_i c_i^{(i\sim m_1)} - i J_{i\sim m_1} \sum_{\mathcal{S} \in \mathcal{S}_{m_1}} c_{m_1}^{(S)} \\ &\quad + f_i^{(i\sim m_1)}, \end{aligned} \quad (3)$$

$$\begin{aligned} \sum_{\substack{\mathcal{S} \in \mathcal{S}_i \\ \mathcal{S} \neq (i\sim m_1)}} \dot{c}_i^{(S)} &= -i\varepsilon_i \sum_{\substack{\mathcal{S} \in \mathcal{S}_i \\ \mathcal{S} \neq (i\sim m_1)}} c_i^{(S)} - i \sum_{\sigma=2}^{n_i} J_{i\sim m_\sigma} \sum_{\mathcal{S} \in \mathcal{S}_{m_\sigma}} c_{m_\sigma}^{(S)} \\ &\quad - f_i^{(i\sim m_1)}. \end{aligned} \quad (4)$$

Only connection $i \sim m_1$ is contained in Eq. (3). Subsequently, if we introduce another auxiliary function $f_i^{(i\sim m_2)}$, the EOM for exclusive connection of $i \sim m_2$ can also be separated from Eq. (4) using the similar procedure. Repeatedly, a series of equations for site i of the whole set of connections, \mathcal{S}_i , are derived,

$$\begin{aligned} \dot{c}_i^{(i\sim m_\sigma)} &= -i\varepsilon_i c_i^{(i\sim m_\sigma)} - i J_{i\sim m_\sigma} \sum_{\mathcal{S} \in \mathcal{S}_{m_\sigma}} c_{m_\sigma}^{(S)} \\ &\quad + f_i^{(i\sim m_\sigma)}, \end{aligned} \quad (5)$$

for $\sigma = 1, \dots, n_i$. Each connection $i \sim m_\sigma$ is associated to a dimerized subsystem. The auxiliary functions $f_i^{(i\sim m_\sigma)}$ for all edges need satisfy the requirement

$$\sum_{\sigma=1}^{n_i} f_i^{(i\sim m_\sigma)} = 0, \quad (6)$$

similar to Kirchhoff's junction rule for DC circuits that the net flow (the sum over all flows for site i) at a junction is zero.

In Eq. (5), the EOMs of n_i local subsystems are exact and no extra assumption is introduced. However, we are still free to choose the form of $c_i^{(S)}$ in the sum in Eq. (5), and the auxiliary functions $f_i^{(i\sim m_\sigma)}$ should be reversely influenced by the choice. Since amplitudes $c_i^{(S)}$ in subsystems are desired to reflect the actual amplitude c_i in the full system, and we also wish to treat the sum with further simplicity, it is natural to impose the assumption

$$c_i^{(i\sim m_1)} = c_i^{(i\sim m_2)} = \dots = c_i^{(i\sim m_{n_i})}. \quad (7)$$

Thus, the relation of amplitudes between the full system and the subsystems is simply $c_i = \sum_{\mathcal{S} \in \mathcal{S}_i} c_i^{(S)} =$

$n_i c_i^{(i \sim m_\sigma)}$ for any of the σ th subsystem. Thereby substituting into Eq. (5) results in

$$\dot{c}_i^{(i \sim m_\sigma)} = -i\varepsilon_i c_i^{(i \sim m_\sigma)} - in_{m_\sigma} J_{i \sim m_\sigma} c_{m_\sigma}^{(i \sim m_\sigma)} + f_i^{(i \sim m_\sigma)}. \quad (8)$$

Besides the outcome of simplified EOMs, the equal distribution of amplitudes $c_i^{(S)}$ in n_i subsystems establishes the matching conditions among subsystems, which is a critical step to find $f_i^{(S)}$. The $n_i - 1$ equations from matching conditions in Eq. (7), together with the junction rule of Eq. (6), can uniquely determine the n_i functions $f_i^{(S)}$.

The above EOMs are derived from the perspective of a single site i for an arbitrary graph. Each equation describes the evolution of a coupling edge $\mathcal{S} = (i \sim m_\sigma) \in \mathcal{S}_i$. Extending the single site to all sites $i \in V$, the above derivation may reversely be viewed from the perspective of edges instead of sites. If sites i and j are connected, it is always possible to select a pair of EOMs for $c_i^{(i \sim j)}$ and $c_j^{(j \sim i)}$ from Eq. (8),

$$\begin{aligned} \dot{c}_i^{(i \sim j)} &= -i\varepsilon_i c_i^{(i \sim j)} - in_j J_{i \sim j} c_j^{(i \sim j)} + f_i^{(i \sim j)}, \\ \dot{c}_j^{(j \sim i)} &= -i\varepsilon_j c_j^{(j \sim i)} - in_i J_{j \sim i} c_i^{(j \sim i)} + f_j^{(j \sim i)}, \end{aligned}$$

which describes the dynamics within subsystem $\mathcal{S} = (i \sim j) = (j \sim i)$. A more compact matrix form is

$$\dot{\mathbf{c}}^{(S)} = -i\mathbf{H}^{(S)} \mathbf{c}^{(S)} + \mathbf{f}^{(S)}, \quad (9)$$

with $\mathbf{c}^{(S)} = (c_i^{(S)}, c_j^{(S)})^T$, the local Hamiltonian

$$\mathbf{H}^{(S)} = \begin{pmatrix} \varepsilon_i & n_j J_S \\ n_i J_S & \varepsilon_j \end{pmatrix}, \quad (10)$$

and the boundary term $\mathbf{f}^{(S)} = (f_i^{(S)}, f_j^{(S)})^T$ accounting for flows via sites in subsystem \mathcal{S} . Although $\mathbf{H}^{(S)}$ is unsymmetric when $n_i \neq n_j$, the hermiticity can still be conserved with a new set of $\mathbf{c}^{(S)}$ by proper linear transformation. When $\mathbf{f}^{(S)} = (0, 0)^T$, Eq. (9) is essentially the Schrödinger equation for the two-level system with the off-diagonal couplings modified by connectivities.

Given the initial condition $\mathbf{c}^{(S)}(0)$, the formal solution of Eq. (9) reads

$$\mathbf{c}^{(S)}(t) = \int_0^t \mathbf{U}^{(S)}(t - \tau) \mathbf{f}^{(S)}(\tau) d\tau + \mathbf{U}^{(S)}(t) \mathbf{c}^{(S)}(0), \quad (11)$$

where $\mathbf{U}^{(S)}(t) = e^{-i\mathbf{H}^{(S)}t}$ is the local time-evolution operator of subsystem \mathcal{S} .

Our aim is to find $\mathbf{f}^{(S)}$ which eventually determines amplitude $\mathbf{c}^{(S)}$. Since Eq. (11) takes the form of a Volterra integral that can be easily analyzed after the Laplace transform,

$$\tilde{\mathbf{c}}^{(S)}(s) = \tilde{\mathbf{U}}^{(S)}(s) [\tilde{\mathbf{f}}^{(S)}(s) + \mathbf{c}^{(S)}(0)], \quad (12)$$

the calculation of $\mathbf{f}^{(S)}$ is actually conducted in the s -domain. Here, variables in the s -domain, as appeared in Eq. (12), are indicated by the tilde. The local time evolution operator $\tilde{\mathbf{U}}^{(S)}(s)$ in the s -domain corresponding to $\mathbf{H}^{(S)}$ in Eq. (10) reads

$$\tilde{\mathbf{U}}^{(S)}(s) = \frac{1}{\Omega^2 + \bar{s}^2} \begin{pmatrix} \bar{s} - i\Delta_{ij} & -in_j J_S \\ -in_i J_S & \bar{s} + i\Delta_{ij} \end{pmatrix} \quad (13)$$

with $\bar{s} = s + i\bar{\varepsilon}$, $\Delta_{ij} = (\varepsilon_i - \varepsilon_j)/2$, $\bar{\varepsilon} = (\varepsilon_i + \varepsilon_j)/2$ and $\Omega = \sqrt{\Delta_{ij}^2 + n_i n_j J_S^2}$.

In the s -domain, the flow function $\mathbf{f}^{(S)}$ can be uniquely determined by solving the linear system generated from both the junction rule Eq. (6) and matching conditions Eq. (7). In Eq. (6), the junction rules are directly expressed as equalities among $f_i^{(S)}$. The explicit form of matching condition Eq. (7), however, assuming site i is shared by both subsystems \mathcal{S} and \mathcal{T} , is given by

$$\begin{aligned} \tilde{u}_{\sigma,1}^{(S)} [\tilde{f}_{i_1}^{(S)} + c_{i_1}^{(S)}(0)] + \tilde{u}_{\sigma,2}^{(S)} [\tilde{f}_{i_2}^{(S)} + c_{i_2}^{(S)}(0)] \\ = \tilde{u}_{\tau,1}^{(T)} [\tilde{f}_{i_1}^{(T)} + c_{i_1}^{(T)}(0)] + \tilde{u}_{\tau,2}^{(T)} [\tilde{f}_{i_2}^{(T)} + c_{i_2}^{(T)}(0)], \end{aligned} \quad (14)$$

where $\tilde{u}_{\sigma(\tau),1(2)}^{(S)}$ is the matrix element of $\tilde{\mathbf{U}}^{(S)}$ in Eq. (13), and $c_i(0)$ is the initial amplitude on site i . Indices $\sigma, \tau = 1, 2$ label the intra-dimer sites, and $i_\alpha^{(S)}$ with $\alpha = 1, 2$ is the actual site index for the α th site in subsystem \mathcal{S} . Note that within the set $\{i_1^{(S)}, i_2^{(S)}, i_1^{(T)}, i_2^{(T)}\}$, two indices must be the same as specified by the matching condition for $\mathcal{S} \neq \mathcal{T}$. Given the unknown flow functions arranged by $\tilde{\mathbf{f}} = (\tilde{\mathbf{f}}^{(a)}, \tilde{\mathbf{f}}^{(b)}, \dots, \tilde{\mathbf{f}}^{(N)})^T$ with the local

flow for subsystem \mathcal{S} , $\tilde{\mathbf{f}}^{(S)} = (\tilde{f}_{i_1}^{(S)}, \tilde{f}_{i_2}^{(S)})^T$, $\tilde{\mathbf{f}}$ can be found by solving the linear system $\tilde{\mathbf{M}}\tilde{\mathbf{f}} = \tilde{\mathbf{b}}$, where $\tilde{\mathbf{M}}$ is the matrix constructed from the matching condition and junction rule. Given an N -site graph with M coupling edges, $\tilde{\mathbf{M}}$ is a $2M \times 2M$ matrix accounting for N equations from junction rules and the rest $2M - N$ equations from matching conditions. The global topology of the graph is encoded in $\tilde{\mathbf{M}}$, whose matrix elements are also embedded with the local properties of subsystems. The array $\tilde{\mathbf{b}}$ is an array formed by all non- $\tilde{f}_i^{(S)}$ terms in Eq. (14) related to initial conditions $c_i(0)$. In the following, the method will be presented in detail with examples.

We note that, in regard to the computational complexity when solving the differential equations, admittedly, our method is not advantageous. Given a homogeneous system of the EOM $i\dot{\mathbf{c}} = \mathbf{H}\mathbf{c}$ with the N -site hamiltonian \mathbf{H} , the typical evaluation of the wavefunctions by $\mathbf{c}(t) = \mathcal{T} e^{-i \int^t dt' \mathbf{H}(t')} \mathbf{c}(0)$ requires one to find the time evolution operator $e^{-i\mathbf{H}\Delta t}$, equivalent to the spectral decomposition $\mathbf{U}^T e^{-i\mathbf{D}\Delta t} \mathbf{U}$. In our method, the diagonalization of \mathbf{H} is not required, since all time evolution operator within the two-level subsystem has a fixed-format closed form solution. Instead, solving the original

Schrödinger equation is recast as treating a series of coupled inhomogeneous two-dimensional matrix equations. The most computationally demanding part is to find the inhomogeneous term $\mathbf{f}_i^{(S)}$ from $\sum_{\{i|\deg(v_i)>1\}} \deg(v_i)$ matching conditions. Usually, the complexity of solving the linear system $\tilde{\mathbf{M}}\tilde{\mathbf{f}} = \tilde{\mathbf{b}}$ is even higher than the exact diagonalization of the original hamiltonian, though the matching matrix is usually sparse because, as suggested by Eq. (14), each row of $\tilde{\mathbf{M}}$ has at most four non-zero elements.

III. APPLICATIONS

A. Flow patterns in diamond graph

In order to show the procedure of the decomposition and obtain the flow patterns, the method is applied to a diamond graph (2-fan including four sites) as shown in Fig. 2(a). The Hamiltonian is $\hat{H} = \sum_i^4 \varepsilon_i |i\rangle\langle i| + J_a|1\rangle\langle 2| + J_b|2\rangle\langle 3| + J_c|3\rangle\langle 4| + J_d|4\rangle\langle 1| + J_e|2\rangle\langle 4| + \text{c.c.}$ and the amplitude on site i of the full system is $c_i(t)$. A diagrammatic representation of the decomposition as shown in Fig. 2(b) allows for the direct translation of Eq. (9) for local EOMs of subsystems $\mathcal{S} \in \{a, b, c, d, e\}$ as followings,

$$\begin{aligned} \begin{pmatrix} \dot{c}_1^{(a)} \\ \dot{c}_2^{(a)} \end{pmatrix} &= -i \begin{pmatrix} \varepsilon_1 & 3J_a \\ 2J_a & \varepsilon_2 \end{pmatrix} \begin{pmatrix} c_1^{(a)} \\ c_2^{(a)} \end{pmatrix} + \begin{pmatrix} f_1^{(a)} \\ f_2^{(a)} \end{pmatrix}, \\ \begin{pmatrix} \dot{c}_2^{(b)} \\ \dot{c}_3^{(b)} \end{pmatrix} &= -i \begin{pmatrix} \varepsilon_2 & 2J_b \\ 3J_b & \varepsilon_3 \end{pmatrix} \begin{pmatrix} c_2^{(b)} \\ c_3^{(b)} \end{pmatrix} + \begin{pmatrix} f_2^{(b)} \\ f_3^{(b)} \end{pmatrix}, \\ \begin{pmatrix} \dot{c}_3^{(c)} \\ \dot{c}_4^{(c)} \end{pmatrix} &= -i \begin{pmatrix} \varepsilon_3 & 3J_c \\ 2J_c & \varepsilon_4 \end{pmatrix} \begin{pmatrix} c_3^{(c)} \\ c_4^{(c)} \end{pmatrix} + \begin{pmatrix} f_3^{(c)} \\ f_4^{(c)} \end{pmatrix}, \\ \begin{pmatrix} \dot{c}_4^{(d)} \\ \dot{c}_1^{(d)} \end{pmatrix} &= -i \begin{pmatrix} \varepsilon_4 & 2J_d \\ 3J_d & \varepsilon_1 \end{pmatrix} \begin{pmatrix} c_4^{(d)} \\ c_1^{(d)} \end{pmatrix} + \begin{pmatrix} f_4^{(d)} \\ f_1^{(d)} \end{pmatrix}, \\ \begin{pmatrix} \dot{c}_2^{(e)} \\ \dot{c}_4^{(e)} \end{pmatrix} &= -i \begin{pmatrix} \varepsilon_2 & 3J_e \\ 3J_e & \varepsilon_4 \end{pmatrix} \begin{pmatrix} c_2^{(e)} \\ c_4^{(e)} \end{pmatrix} + \begin{pmatrix} f_2^{(e)} \\ f_4^{(e)} \end{pmatrix}, \end{aligned} \quad (15)$$

where $c_i^{(S)}$ is the amplitude in subsystem. According to matching conditions, we have relations of amplitudes between subsystems and the full system, $c_i^{(S)} = c_i/2$ for $i = 1, 3$ and $c_i^{(S)} = c_i/3$ for $i = 2, 4$.

Next we show how flow functions in Eq. (15) of the form $\tilde{\mathbf{f}} = (\tilde{\mathbf{f}}^{(a)}, \tilde{\mathbf{f}}^{(b)}, \tilde{\mathbf{f}}^{(c)}, \tilde{\mathbf{f}}^{(d)}, \tilde{\mathbf{f}}^{(e)})^T = (\tilde{f}_1^{(a)}, \tilde{f}_2^{(a)}, \tilde{f}_2^{(b)}, \tilde{f}_3^{(b)}, \tilde{f}_3^{(c)}, \tilde{f}_4^{(c)}, \tilde{f}_4^{(d)}, \tilde{f}_1^{(d)}, \tilde{f}_2^{(e)}, \tilde{f}_4^{(e)})^T$ are determined. As in Eq. (7), the six restricting equalities, $c_1^{(a)} = c_1^{(d)}$, $c_2^{(a)} = c_2^{(b)} = c_2^{(e)}$, $c_3^{(b)} = c_3^{(c)}$ and $c_4^{(c)} = c_4^{(d)} = c_4^{(e)}$, are imposed by matching conditions. Together with the four equations from the junction rules, $f_1^{(a)} + f_1^{(d)} = 0$, $f_2^{(a)} + f_2^{(b)} + f_2^{(d)} = 0$, $f_3^{(b)} + f_3^{(c)} = 0$ and

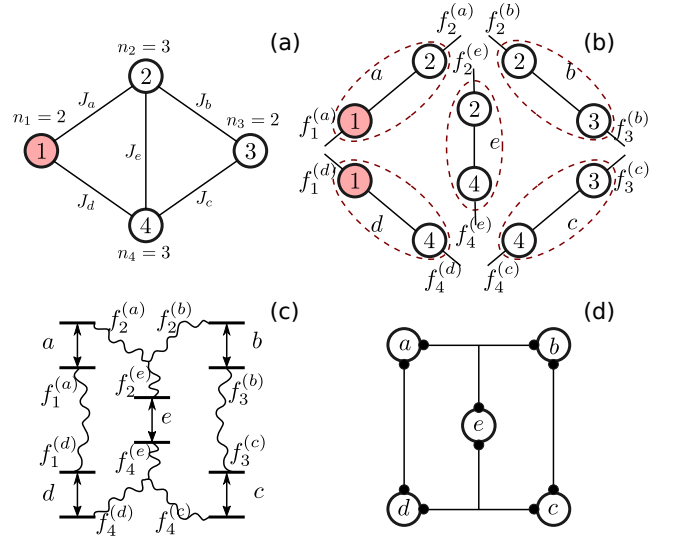


Figure 2. (a) A four-site diamond graph. The initial state is on site $|1\rangle$ labeled in red. (b) The decomposition of the graph according to the coupling edges into subsystems as indicated by dashed circles. The flow functions $f_i^{(S)}$ are labeled by the double ends of each subsystem. (c) Alternatively, each subspace as a two-level system represents a qubit subject to perturbing flows on the two internal states. (d) The dimerized decomposition is equivalent to swapping the roles of sites and edges in panel (a), and now we focus on the central role of edges in the original graph. Each site (circle) is a dimerized subspace, whose internal sites are perturbed by auxiliary flows represented by a pair of black dots.

$f_4^{(c)} + f_4^{(d)} + f_4^{(e)} = 0$, we construct the matrix $\tilde{\mathbf{M}}$ (see Appendix for the explicit form) from which the ten flow functions can be determined by solving $\tilde{\mathbf{f}} = \tilde{\mathbf{M}}^{-1}\tilde{\mathbf{b}}$.

Taking the simplest case with all edges of identical coupling strength J for instance, solving the determinant equation $|\tilde{\mathbf{M}}(s)| = 0$ shows the k th zero is given by $s_k^{(p)} \in iJ\{-\frac{1}{2}(\sqrt{17}+1), 0, 1, \frac{1}{2}(\sqrt{17}-1)\}$. Since $\tilde{\mathbf{f}} = \tilde{\mathbf{M}}^{-1}\tilde{\mathbf{b}}$, $s_k^{(p)}$ is a pole of $\tilde{\mathbf{f}}$ in the complex s -plane. Clearly, the relation between the k th pole with the eigenvalue λ_k obtained using spectral method is given by $\lambda_k = is_k^{(p)}$.

Given a subsystem \mathcal{S} , from Eq. (12) it is clearly seen that the amplitude $\tilde{c}^{(S)}$, as a vector spanned in the basis of the local subsystem, can be obtained from the driving source $\tilde{\mathbf{f}}^{(S)}$ in Eq. (12) followed by the vector operation of the local time evolution $\tilde{\mathbf{U}}^{(S)}$. Usually, only poles of $\tilde{c}^{(S)}$ in the s -plane, which are equivalent to the poles of $\tilde{\mathbf{f}}^{(S)}$, contributes to $c^{(S)}$ in the time domain. The poles are typically directly derived from the zeros of the characteristic polynomial $|\tilde{\mathbf{M}}(s)|$. But one should note that the value that renders any matrix element of $\tilde{\mathbf{M}}$ singular and coincides with any eigenvalue of $\tilde{\mathbf{U}}^{(S)}$ is also a pole. For each pole $s_k^{(p)}$, the real and imaginary parts represent the decay rate and oscillation frequency, respectively. It

corresponds to an eigenmode of λ_k or a path in the spectral method. The amplitude $\mathbf{c}^{(S)}$ is the superposition of components over all these modes. Each as a mode should present a distribution chart of $\text{Res}_{s_k^{(p)}} \tilde{f}_i$ as illustrated in Fig. 2(b). Here, $\text{Res}_{s_k^{(p)}} \tilde{f}_i$ is the residue of \tilde{f}_i for the k th pole $s_k^{(p)} = -i\lambda_k$.

Although the system can be analyzed with the spectral method as well, the added values of the method is that it provides a different perspective to view the quantum evolution based on edges of a graph. Conventionally, sites or vertices are considered the primitive and one typically focuses on the evolution of components of sites. Here, however, edges are viewed as taking the central role, as shown in Fig. 2(d). The subspace, consisting of a pair of sites and the coupling edge, is a two-level qubit that is the smallest nontrivial local system [Fig. 2(c)] with tremendously wide applications. Unlike a usual isolated two-level system, however, states i and j of \mathcal{S} are allowed to be perturbed by auxiliary functions $f_i^{(S)}(t)$ and $f_j^{(S)}(t)$, respectively. As depicted by the matching condition, $f_i^{(S)}$ is not arbitrarily but necessarily introduced to tune the amplitudes in the local qubit to be consistent with the ones in the original network. Since $f_i^{(S)}$ can be uniquely determined once the topology and parameters of the network is given, it is characteristic of the dynamics on the network.

An intuitive way to understand the role of $f_i^{(S)}$ is to visualize the distribution over all sites and edges on the graph. In the time domain, $f_i^{(S)}(t)$ being a time-dependent continuous function is difficult to present for a static image of the network, therefore it is helpful to switch to the s -domain and seek for an appropriate representation. In fact, as the amplitude of site i is given by $c_i(t) = \sum_k C_{i,k} e^{-i\lambda_k t}$ for $\lambda_k = i s_k^{(p)}$ with k over all eigenmodes, only a finite numbers of $s_k^{(p)}$ contribute to the wave function after transforming back to the time domain. However, since $f_i^{(S)}(s)$ at a pole is singular, the distribution of $\chi_{i,k}^{(S)} \equiv \text{Res}_{s \rightarrow s_k^{(p)}} f_i^{(S)}(s)$ is instead shown on the graph.

For the k th eigenvalue $\lambda_k = i s_k^{(p)}$, defining the vector $\mathbf{C}_k^{(S)} \equiv (C_{i,k}, C_{j,k})^T$ for the pair of sites within $\mathcal{S} = i \sim j$, it is shown from Eq. (12) that

$$\mathbf{C}_k^{(S)} = \text{Res}_{s \rightarrow s_k^{(p)}} \tilde{\mathbf{c}}^{(S)}(s) = \tilde{\mathbf{U}}^{(S)}(s_k^{(p)}) \boldsymbol{\chi}_k^{(S)}, \quad (16)$$

where $\boldsymbol{\chi}_k^{(S)} \equiv \text{Res}_{s \rightarrow s_k^{(p)}} \tilde{\mathbf{f}}^{(S)}(s)$. In other words, coefficient $\mathbf{C}_k^{(S)}$ is the response of the local evolution operator $\tilde{\mathbf{U}}^{(S)}(s_k^{(p)})$ to the whole network determined perturbing source $\boldsymbol{\chi}_k^{(S)}$. Eq. (16) effectively separates the influence of the global network outside the local system from the one within the local system. Especially when $\tilde{\mathbf{U}}^{(S)}(s_k^{(p)})$ of the studied subsystem remains untouched, it allows one to trace how $\mathbf{C}_k^{(S)}$ is affected solely by the global

network determined $\boldsymbol{\chi}_k^{(S)}$.

The visualization of both contributions from $\tilde{\mathbf{U}}^{(S)}(s_k^{(p)})$ and $\boldsymbol{\chi}_k^{(S)}$ over all sites and edges are shown in Fig. 3. With full definitions listed in the caption of the figure, the corresponding vectors are redefined by $\mathbf{u}_{i,k}^{(S)}$ and $\boldsymbol{\chi}_{i,k}^{(S)}$ for site i , edge \mathcal{S} and eigenmode k . The vectors show the separation of the internal influence of the local subspace from the external one outside the subspace. The vectors for eigenmode λ_k can be easily compared among all sites on different edges. The magnitude of vector $\boldsymbol{\chi}_{i,k}^{(S)}$ represents the influence from the global network imposing on the subspace. As for the directions of vectors $\mathbf{u}_{i,k}^{(S)}$ and $\boldsymbol{\chi}_{i,k}^{(S)}$, if subspace \mathcal{S} includes sites i and j , the larger the horizontal component of a vector, the larger the contribution from the studied site i ; while the larger the component in the vertical direction, the larger the contribution from the other site j . The direction of vectors may help define the phase within the subsystem to study the change with parameters. Due to the junction rule, $\sum_{\mathcal{S}} \boldsymbol{\chi}_{i,k}^{(S)} = 0$, for site i the sum over horizontal components of $\boldsymbol{\chi}_{i,k}^{(S)}$ for different \mathcal{S} is zero.

The separation of the contributions may be examined from two perspectives. On one hand, when all parameters (e.g., site energies and coupling strengths) are identical, the distribution of vectors characterizes the influence of global topology on the quantum evolution of the nearest neighboring environment. When the network structure is fixed, on the other hand, if some local property is altered, the distribution informs how the change of parameters perturbs local subsystems. Here, we present the analysis following the guideline: Fig. 3(a)-(d) show the distribution of vectors for the diamond graphs with all parameters identical, while (e)-(h) are results when the graph is perturbed by changing $J_a = 1.5$.

Vector $\mathbf{u}_{i,k}^{(S)}$ reveals local properties within the subspace. Especially, as shown in Fig. 3(a)-(d), when $J_{\mathcal{S}} = 1$ for all edges and the whole network is symmetric along sites 1-2-3 and 1-4-3, vectors $\mathbf{u}_{2,k}^{(b)}$, $\mathbf{u}_{3,k}^{(c)}$, $\mathbf{u}_{2,k}^{(a)}$ and $\mathbf{u}_{3,k}^{(d)}$ are identical due to the same local properties within subspaces $\mathcal{S} = a, b, c$ and d . Similarly, $\mathbf{u}_{2,k}^{(e)}$ and $\mathbf{u}_{3,k}^{(e)}$ are also the same in subspace e . But the latter two vectors differ from the former because of the difference of connectivities, reflecting properties of individual local subspaces.

The local properties of subspaces, including site energies, connectivities, and the coupling strength, determine $\mathbf{u}_{i,k}^{(S)}$. Though the coupling strength in $\mathcal{S} = a$ is changed in Fig. 3(e)-(h), the vectors outside \mathcal{S} , like $\mathbf{u}_{2,k}^{(b)}$, $\mathbf{u}_{3,k}^{(c)}$ and $\mathbf{u}_{3,k}^{(d)}$, $\mathbf{u}_{4,k}^{(b)}$ and $\mathbf{u}_{4,k}^{(c)}$, $\mathbf{u}_{2,k}^{(e)}$ and $\mathbf{u}_{3,k}^{(e)}$ are still identical because of the same local environments. The vectors are only slightly changed when $J_a = 1 \rightarrow J_a = 1.5$ by different eigenvalues. While vectors within a , $\mathbf{u}_{1,k}^{(a)}$ and $\mathbf{u}_{2,k}^{(a)}$, change dramatically.

Vector $\boldsymbol{\chi}_{i,k}^{(S)}$ denotes the global influence of the whole network on the local subspace. For some eigenmode, e.g.,

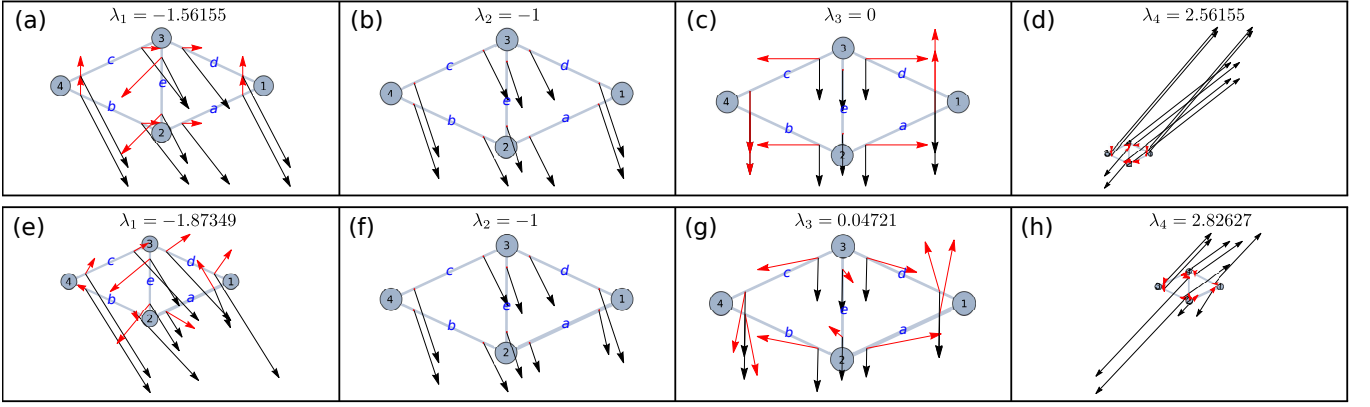


Figure 3. Distribution of vectors that separate the local response from the global-network induced perturbation in the diamond graph of Fig. 2. Panels (a)-(d) ordered by eigenvalues λ_k from lower to higher values show the distribution when coupling strengths are all $J_S = 1$. On all sites $\{i\}$ and edges $\{S\}$, vectors $\mathbf{u}_{i,k}^{(S)}$ (black arrow) and $\chi_{i,k}^{(S)}$ (red arrow) represent contributions from local evolution operator and perturbing flow, respectively. The vectors are defined as followings: If site i is the first site within \mathcal{S} , we define $\mathbf{u}_{i,k}^{(S)} = [\tilde{u}_{1,1}^{(S)}(s_k^{(p)}), \tilde{u}_{1,2}^{(S)}(s_k^{(p)})]$. Otherwise, if site i is treated as the second site in \mathcal{S} , $\mathbf{u}_{i,k}^{(S)} = [\tilde{u}_{2,2}^{(S)}(s_k^{(p)}), \tilde{u}_{2,1}^{(S)}(s_k^{(p)})]$. Similarly, the vector of the perturbing source at site i is defined by $\chi_{i,k}^{(S)} = [\chi_{i,k}^{(S)}, \chi_{j,k}^{(S)}]$ if \mathcal{S} has two sites i and j . The above definitions always render the studied site as the first element that plays the central role. Vectors $\mathbf{u}_{i,k}^{(S)}$ and $\chi_{i,k}^{(S)}$ are labeled on each edge \mathcal{S} around site i . Moreover, as Eq. (16) suggests, the coefficient of the wave function can be read directly from the inner product of the pair of $\mathbf{u}_{i,k}^{(S)}$ and $\chi_{i,k}^{(S)}$ (projection from black arrow to the red arrow). Panels (e)-(g) show the vector distributions when $J_a = 1.5$ while all other edges remain $J_S = 1$ for $\mathcal{S} \neq a$.

Fig. 3(b) when $\lambda = -1$, $\chi_{i,k}^{(S)}$ is zero and subsystem \mathcal{S} is isolated from the whole network. While when $\chi_{i,k}^{(S)}$ is significant, it indicates that the environment outside the subspace \mathcal{S} should have considerable impact. $\chi_{i,k}^{(S)}$ usually varies when parameters of the network change. As shown in Fig. 3(e)-(h) when J_a increases, all vectors rotate to a certain extent. If local properties of subspace are not altered, e.g., internal properties in subspace c are intact when J_a increases, the change within the subspace, $\chi_{3,k}^{(c)}$ and $\chi_{4,k}^{(c)}$, are only induced by the change of the global network. The distributions also show the dependence of $\chi_{i,k}^{(S)}$ on J_S . The magnitudes of $\chi_{1,k}^{(a)}$ and $\chi_{2,k}^{(a)}$ within subspace a increase with J_S , while lengths of $\chi_{i,k}^{(S)}$ in other subspaces are not changed dramatically. In addition, the vectors in Fig. 3(a)-(d) exhibit symmetric distribution along site 1-4-3 and 1-2-3, indicating the system can be further reduced to a three-site linear chain. While in Fig. 3(e)-(h) when $J_a = 1.5$ the symmetry of the distribution of $\chi_{i,k}^{(S)}$ is broken and the system is irreducible.

The distribution shown in Fig. 3 has extra significance besides the separation of local and global properties. In Eq. (16), $C_{i,k} = \mathbf{u}_{i,k}^{(S)} \chi_{i,k}^{(S)}$ allows one to read the component of wave function of each site directly from the inner product of vectors $\mathbf{u}_{i,k}^{(S)}$ and $\chi_{i,k}^{(S)}$. Since the matching condition assumes the equivalent $C_{i,k}$ shared among subspaces, we may choose a pair of vectors arbitrarily in any involved subspace \mathcal{S} . The vectors help identify immediately all zero components that do not contribute to

the amplitude of a specific site. In Fig. 3(b), $\chi_{i,2}^{(S)}$ being zero vector leads to $C_{i,2} = 0$ for all sites when $\lambda_2 = -1$. In Fig. 3(c), vectors $\mathbf{u}_{3,3}^{(S)}$ and $\chi_{3,3}^{(S)}$ for site 3 being orthogonal also results in $C_{3,3} = 0$. While when $J_a = 1.5$ as shown in Fig. 3(g), $\chi_{3,3}^{(S)}$ rotates slightly and $C_{3,3}$ is no longer zero due to the breaking of the orthogonality.

Thereby, when parameters are altered, the change of all vectors separated by local and global contributions can be simultaneously traced on the graph, and the wave functions can be easily determined. It offers the possibility to design and manipulate the vectors to control the quantum evolution on the graph for optimized quantum state transfer.

B. Transport efficiency in trimer

In this section, the trimer model is examined with the dimerized decomposition. The trimer model has the potential application to optimize the excitation energy transfer via biomolecular network, e.g., the excitation transfer from B800 to B850 bacteriochlorophylls (BChls) in light-harvesting complex II (LH2). With the structure dimerization of the B850 ring [22–24], a trimer can be viewed as a subunit of the two-layer rings, between which a carotenoid connects B800 BChl (source) with one of the two B850 BChls (traps). The excitation transport from a source site to the two-site traps within the single-exciton manifold can be investigated with the trimer as shown in Fig. 4(a).

The trimer has the source of the excitation energy

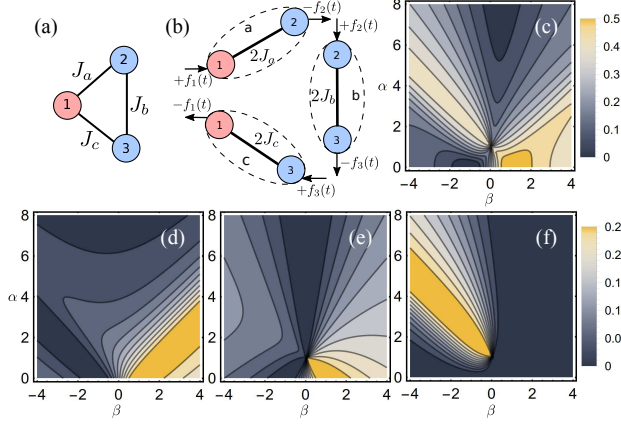


Figure 4. The dimerized decomposition scheme. (a) A closed-loop trimer (K_3 graph) is decomposed into (b) a set of subsystems (dashed circles), each of which consists of two sites, and subsystems communicate via flows f_i (arrows). The initial excitation starts from site 1 (red), and sites 2 and 3 are targets (blue). Panel (c) shows the efficiency distribution $\eta_2(\beta, \alpha)$. Panels (d)-(f) show the partial contributions of path m as introduced in Eq. (19).

at site 1, and the target sites 2 and 3 are supposed to trap the energy. For simplicity, the on-site energies ε_i

and decoherence rates Γ_i are assumed identical for all sites. Coupling strengths among three sites, J_a , J_b and J_c , are adjustable, e.g., by changing spatial distances between the sites. The Hamiltonian for the trimer system is $\hat{H} = \sum_i^3 \varepsilon_i |i\rangle\langle i| + J_a |1\rangle\langle 2| + J_b |2\rangle\langle 3| + J_c |3\rangle\langle 1| + \text{c.c.}$. Here we use the dimerized decomposition to calculate the amplitudes. The decomposition is shown in Fig. 4(b) with the EOMs of subsystems determined by Eq. (9). The amplitudes $\mathbf{c}^{(S)}$ are $\mathbf{c}^{(a)} = (c_1^{(a)}, c_2^{(a)})^T$, $\mathbf{c}^{(b)} = (c_2^{(b)}, c_3^{(b)})^T$ and $\mathbf{c}^{(c)} = (c_3^{(c)}, c_1^{(c)})^T$. Note that since $n_i = 2$ for all sites in the K_3 graph, the amplitude in the full system c_i is evenly distributed in the subsystems, $c_i^{(S)} = c_i/2$. Accordingly, the initial conditions are $\mathbf{c}^{(a)}(0) = (1/2, 0)^T$, $\mathbf{c}^{(b)}(0) = (0, 0)^T$ and $\mathbf{c}^{(c)}(0) = (0, 1/2)^T$. Using the junction rule, it is convenient to directly define $\mathbf{f} = (\mathbf{f}^{(a)}, \mathbf{f}^{(b)}, \mathbf{f}^{(c)})^T$ with $\mathbf{f}^{(a)} = (f_1, -f_2)^T$, $\mathbf{f}^{(b)} = (f_2, -f_3)^T$ and $\mathbf{f}^{(c)} = (f_3, -f_1)^T$. Assuming $\varepsilon_i = 0$, the local Hamiltonian of subsystem S is $\mathbf{H}^{(S)} = 2J_S \begin{pmatrix} 0 & 1 \\ 1 & 0 \end{pmatrix}$.

Substituting $\mathbf{H}^{(S)}$, $\mathbf{c}^{(S)}$ and $\mathbf{f}^{(S)}$ into Eq. (9), we obtain the EOMs of all subsystems.

The matching conditions in the s -domain, $\tilde{c}_2^{(a)} = \tilde{c}_2^{(b)}$, $\tilde{c}_3^{(b)} = \tilde{c}_3^{(c)}$ and $\tilde{c}_1^{(c)} = \tilde{c}_1^{(a)}$, yield the linear system with respect to \tilde{f}_i ,

$$\begin{pmatrix} -\tilde{u}_{22}^{(c)} - \tilde{u}_{11}^{(a)} & \tilde{u}_{12}^{(a)} & \tilde{u}_{21}^{(c)} \\ \tilde{u}_{21}^{(a)} & -\tilde{u}_{22}^{(a)} - \tilde{u}_{11}^{(b)} & \tilde{u}_{12}^{(b)} \\ \tilde{u}_{12}^{(c)} & \tilde{u}_{21}^{(b)} & -\tilde{u}_{22}^{(b)} - \tilde{u}_{11}^{(c)} \end{pmatrix} \begin{pmatrix} \tilde{f}_1 \\ \tilde{f}_2 \\ \tilde{f}_3 \end{pmatrix} = \begin{pmatrix} \frac{1}{n_1} [-\tilde{u}_{22}^{(c)} + \tilde{u}_{11}^{(a)}] \\ -\frac{1}{n_1} \tilde{u}_{21}^{(a)} \\ \frac{1}{n_1} \tilde{u}_{12}^{(b)} \end{pmatrix}, \quad (17)$$

where $\tilde{u}_{ij}^{(S)}$ is the element of $\tilde{\mathbf{U}}^{(S)} = \frac{1}{4J_s^2 + s^2} \begin{pmatrix} s & -2iJ_s \\ -2iJ_s & s \end{pmatrix}$ reduced from Eq. (13). Solving Eq. (17) yields

$$\begin{aligned} \tilde{f}_1(s) &= \frac{s(J_a^2 - J_c^2)}{g(s)}, \\ \tilde{f}_2(s) &= \frac{sJ_cJ_b - iJ_a(s^2 + 2J_b^2)}{g(s)}, \\ \tilde{f}_3(s) &= -\frac{sJ_aJ_b - iJ_c(s^2 + 2J_b^2)}{g(s)} \end{aligned} \quad (18)$$

with $g(s) = 2[s^3 + (J_a^2 + J_b^2 + J_c^2)s - 2iJ_aJ_bJ_c]$ the characteristic polynomial. Note that $\tilde{f}_2(s)$ and $\tilde{f}_3(s)$ differ by exchanging subscripts a and c since they are treated on the equal footing within subsystem b . The signs of $\tilde{f}_2(s)$ and $\tilde{f}_3(s)$ also differ due to the definitions as the flow-in and flow-out, respectively. By applying the inverse

Laplace transform, we obtain

$$\begin{aligned} f_1(t) &= -\frac{i}{2} \sum_m \frac{(J_a^2 - J_c^2)\lambda_{m_1}}{(\lambda_{m_1} - \lambda_{m_2})(\lambda_{m_1} - \lambda_{m_3})} e^{i\lambda_{m_1}t}, \\ f_2(t) &= -\frac{i}{2} \sum_m \frac{J_bJ_c\lambda_{m_1} + J_a(\lambda_{m_1}^2 - 2J_b^2)}{(\lambda_{m_1} - \lambda_{m_2})(\lambda_{m_1} - \lambda_{m_3})} e^{i\lambda_{m_1}t}, \end{aligned} \quad (19)$$

where the integer index m_i is the i th member of m , the member of a cyclically ordered set, i.e., $(m_1, m_2, m_3) \in \{(1, 2, 3), (2, 3, 1), (3, 1, 2)\}$. λ_j are zeros of $g(i\lambda)$ whose solutions are $\lambda_j \in 2\kappa\{-\cos(\theta/3), \cos[(\theta - \pi)/3], \cos[(\theta + \pi)/3]\}$ with $\kappa = [(J_a^2 + J_b^2 + J_c^2)/3]^{1/2}$ and $\theta = \arg[J_aJ_bJ_c + i[\kappa^6 - (J_aJ_bJ_c)^2]^{1/2}]$. $f_3(t)$ can also be obtained by exchanging subscripts a and c in $-f_2(t)$. It is shown that the zeros satisfy $\sum_j \lambda_j = 0$. Moreover, $\theta = \arctan[(J_a^2 + J_b^2 + J_c^2)^3 / (3^3 J_a^2 J_b^2 J_c^2) - 1]^{1/2}$ with $\kappa^6 - (J_aJ_bJ_c)^2 \geq 0$. Breaking any edge, e.g., $J_a = 0$, results in $\theta = \pi/2$ and $\lambda_j \in \{-\sqrt{3}, \sqrt{3}, 0\}\kappa$. In addition, if $J_a^2 = J_b^2 = J_c^2$, we have $\theta = 0$ and degeneracy occurs as $\lambda_j \in \{-2, 1, 1\}\kappa$.

Substituting $\tilde{\mathbf{U}}^{(S)}(s)$, $\tilde{\mathbf{f}}^{(S)}(s)$ and $\mathbf{c}^{(S)}(0)$ into Eq. (12)

we find $\tilde{c}_1(s) = (s^2 + J_b^2)/g(s)$ and $\tilde{c}_2(s) = (isJ_a + J_bJ_c)/g(s)$. The amplitude $\tilde{c}_3(s)$ is similar to $\tilde{c}_2(s)$ differing by exchanging a and c . Back to the time domain, the amplitudes of sites 1 and 2 are $c_i(t) = \frac{1}{2} \sum_m C_i^{(m)} e^{i\lambda_{m_1} t}$, ($i = 1, 2$) with

$$C_1^{(m)} = \frac{\lambda_{m_1}^2 - J_b^2}{(\lambda_{m_1} - \lambda_{m_2})(\lambda_{m_1} - \lambda_{m_3})},$$

$$C_2^{(m)} = \frac{J_a\lambda_{m_1} - J_bJ_c}{(\lambda_{m_1} - \lambda_{m_2})(\lambda_{m_1} - \lambda_{m_3})}. \quad (20)$$

The above derivation assumes that $\bar{\varepsilon} = 0$. If the decoherence rate Γ is considered for each site [9], $\bar{\varepsilon} = -i\frac{\Gamma}{2}$. Accordingly, $s \rightarrow s + \frac{\Gamma}{2}$ in Eq. (18), and in $f_i(t)$ and $c_i(t)$, $e^{i\lambda_k t} \rightarrow e^{i\lambda_k t - \Gamma t/2}$.

We apply the method to calculate the excitation transfer efficiency η_i toward site i and its dependence on J_S and Γ . The efficiency is defined by $\eta_i = \lim_{t \rightarrow \infty} [\sigma_i(t) / \sum_j \sigma_j(t)]$ with $\sigma_i(t) = \int_0^t d\tau |c_i(\tau)|^2$ the accumulated population trapped at site i by time t . With the denominator $\sum_j \sigma_j(\infty) = 1/\Gamma$, we have $\eta_i = \Gamma \sigma_i(\infty)$. Substituting $c_i(t) = n_i c_i^{(S)}(t) = \sum_m C_i^{(m)} e^{i\lambda_{m_1} t - \Gamma t/2}$ into η_i , we find $\eta_i = \Gamma \sum_{m,n} (C_i^{(m)})^* C_i^{(n)} / [i(\lambda_{m_1} - \lambda_{n_1}) + \Gamma]$. With $\lambda_{m_1}, C_i^{(m)} \in \mathbb{R}$, the efficiency is given by

$$\eta_i = \sum_m |C_i^{(m)}|^2 + 2 \sum_{m < n} \frac{C_i^{(m)} C_i^{(n)}}{1 + [(\lambda_{m_1} - \lambda_{n_1})/\Gamma]^2}, \quad (21)$$

with the first non-interfering sum and the last interfering part. The ratio between $(\lambda_{m_1} - \lambda_{n_1})$ and Γ decides the contribution of the interfering part to η_i . When Γ is small, the interfering term vanishes and $\eta_i \rightarrow \sum_m |C_i^{(m)}|^2$. On the other hand, the contribution of interference increases with Γ . When $\Gamma \rightarrow \infty$, $\eta_i = \sum_{m < n} |C_i^{(m)} + C_i^{(n)}|^2$ approaches the limit when the decoherence induced destructive interference dominates and η_2 is low in general.

The efficiency of excitation transfer toward site 2, η_2 , is evaluated by substituting $C_2^{(m)}$ in Eq. (20) into Eq. (21). Alternatively, η_i can be analyzed using $\tilde{c}_i(s)$ in the s -domain without the necessity of the inverse Laplace transform back to the time domain, because the relevant information is embedded in poles of m , and the $C_i^{(m)}$ is exactly the residues of $\tilde{c}_i(s)$ in the complex s -plane.

By introducing two dimensionless parameters α and β , we define $J_a = (1 + \beta)J$, $J_c = (1 - \beta)J$ and $J_b = \alpha J$. The parameter β describes the asymmetry for the upper and lower source-trap couplings, and α accounts for the inter-trap coupling. In the LH2 complex, α characterizes the dimerization of the B850 BChl ring that tunes the coupling J_b between neighboring B850 BChls, and β , as the difference between J_a and J_c , describes the spatial deformation when rotating the B850 ring relative to the B800 ring [23].

The efficiency $\eta_2(\beta, \alpha)$ is shown in Fig. 4(b) for $\Gamma = 0.01J$ with the distinct negative- and positive- β

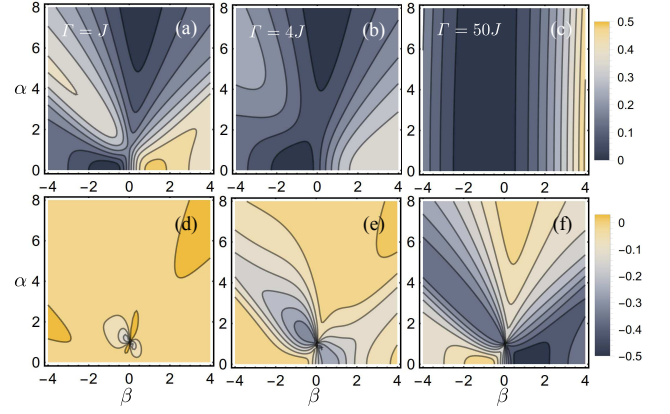


Figure 5. Efficiencies $\eta_2(\beta, \alpha)$ for $\Gamma = J, 4J$ and $50J$ are shown in panels (a)-(c), respectively. In panel (c) for $\Gamma = 50J$, the value of η_2 is low and hence multiplied by a factor 25 to highlight the distribution. The corresponding partial contributions from the interfering part in Eq. (21) are shown in panels (d)-(f).

distributions. In the negative- β region, the excitation is transferred mostly via the indirect path $1 \leftrightarrow 3 \leftrightarrow 2$, whereas in the positive- β region the direct path $1 \leftrightarrow 2$ dominates the contribution. Changing the positivity of β adjusts the ratio of contributions from direct and indirect paths. The global maximum of η_2 present in the positive- β region suggests the transfer of high efficiency should favor the direct path.

When $\beta = 1$, the indirect path is completely blocked. At $(\beta, \alpha) = (1, 0)$, the maximal $\eta_2 = 1/2$ is obtained and the excitation is transferred via $1 \leftrightarrow 2$ directly. When $\beta = -1$, the direct path is blocked instead and the transfer depends only on the indirect path $1 \leftrightarrow 3 \leftrightarrow 2$. Particularly when $\alpha = 0$, site 2 is isolated and $\eta_2 = 0$. Either via direct or indirect path, the high- η_2 distribution is roughly along $\beta = 1 + |\alpha|$ when $\Gamma \ll J$.

When $\beta = 0$, the identical paths $1 \leftrightarrow 2$ and $1 \leftrightarrow 3$ render sites 2 and 3 a single effective site with the α -tunable energy levels. When $\alpha = 0$, the energy of the effective site is ε_1 . Increasing α , however, the energy level splits leading to an increasingly large energy gap with the center moving away from ε_1 that lowers η_2 . When the system is symmetric as $J_a = J_b = J_c$, i.e., $(\beta, \alpha) = (0, 1)$, the degeneracy occurs and $\eta_2 = 1/3$.

Since η_2 depends almost on the non-interfering part when $\Gamma < J$, we show in Fig. 4(d)-(f) the partial contributions from $|C_2^{(m)}|^2$. Roughly, $m = (1, 2, 3)$ and $(2, 3, 1)$ correspond to the direct paths and $m = (3, 1, 2)$ the indirect path. Each path contributes $\sim 1/4$ to the efficiency, and the maximum $\eta_2 = 1/2$ is when the partial contributions of direct paths, Fig. 4(d) and (e), overlap at $(\beta, \alpha) = (1, 0)$.

Fig. 5(a) confirms that η_2 is dominated by the non-interfering sum of $|C_2^{(m)}|^2$ when $\Gamma < J$, as depicted in Eq. (21), which also indicates the non-interfering part is Γ irrelevant, as shown by the similar patterns in Fig. 4(c)

and Fig. 5(a). In Fig. 5(c) when $\Gamma \gg J$, however, the interfering part plays an increasingly important role and η_2 becomes Γ -dependent. Increasing Γ , the maximum of η_2 , which is located at $(\beta, \alpha) = (1, 0)$ when $\Gamma < J$, moves outward along the β -axis. It suggests that the efficiency is deteriorated by dissipations on all sites and a stronger coupling J_b is in need for the maximized efficiency. The origin of the low η_2 when $\Gamma \gg J$ is due to the negative contribution from the interfering part, as shown in Fig. 5(d)-(f). Being negative, the interfering part intensifies with increasing Γ until its distribution resembles the non-interfering part, which is neutralized by the former yielding the low η_2 .

In summary, we have introduced the method of dimerized decomposition to study the quantum evolution on a graph. The method allows for the separation of the local subsystems from the global network and offers insights from the perspective of perturbing flows among sites. The decomposition is applied to a diamond graph for demonstration, and the EOMs can be easily generated using the diagrammatic technique. The method allows for observing the distribution of vectors representing influences from the local time evolution and the perturbation from the global network. Furthermore, we apply the method to analyze the model of a source-trap-trap

trimer, on which the excitation transfer efficiency influenced by the symmetry of source-trap couplings and the inter-trap coupling is investigated. With contributions from direct and indirect paths separated, the transfer efficiency is deteriorated by decoherence-induced destructive interference. Beyond examples we have shown in this work, the dimerized decomposition is universal and straightforward for further extensions towards arbitrary graphs. Besides applications to study the transport efficiency, as the graph presented here mapping the state-to-state transition, the relation between the local subsystem and global network may provide the measurement to better understand concepts like entanglement in multi-particle quantum systems.

APPENDIX

In Sec. III A for the diamond graph, the flow functions need to be determined by solving the linear system $\tilde{\mathbf{M}}\tilde{\mathbf{f}} = \tilde{\mathbf{b}}$. Given flow functions of the order $\tilde{\mathbf{f}} = (\tilde{f}_1^{(a)}, \tilde{f}_2^{(a)}, \tilde{f}_2^{(b)}, \tilde{f}_3^{(b)}, \tilde{f}_3^{(c)}, \tilde{f}_4^{(c)}, \tilde{f}_4^{(d)}, \tilde{f}_1^{(d)}, \tilde{f}_2^{(e)}, \tilde{f}_4^{(e)})^T$, the 10×10 matrix $\tilde{\mathbf{M}}$ constructed from both the junction rules and the matching conditions reads

$$\tilde{\mathbf{M}} = \begin{pmatrix} \tilde{u}_{1,1}^{(a)} & \tilde{u}_{1,2}^{(a)} & 0 & 0 & 0 & 0 & -\tilde{u}_{2,1}^{(d)} & -\tilde{u}_{2,2}^{(d)} & 0 & 0 \\ \tilde{u}_{2,1}^{(a)} & \tilde{u}_{2,2}^{(a)} & -\tilde{u}_{1,1}^{(b)} & -\tilde{u}_{1,2}^{(b)} & 0 & 0 & 0 & 0 & 0 & 0 \\ \tilde{u}_{2,1}^{(a)} & \tilde{u}_{2,2}^{(a)} & 0 & 0 & 0 & 0 & 0 & 0 & -\tilde{u}_{1,1}^{(e)} & -\tilde{u}_{1,2}^{(e)} \\ 0 & 0 & \tilde{u}_{2,1}^{(b)} & \tilde{u}_{2,2}^{(b)} & -\tilde{u}_{1,1}^{(c)} & -\tilde{u}_{1,2}^{(c)} & 0 & 0 & 0 & 0 \\ 0 & 0 & 0 & 0 & \tilde{u}_{2,1}^{(c)} & \tilde{u}_{2,2}^{(c)} & -\tilde{u}_{1,1}^{(d)} & -\tilde{u}_{1,2}^{(d)} & 0 & 0 \\ 0 & 0 & 0 & 0 & \tilde{u}_{2,1}^{(c)} & \tilde{u}_{2,2}^{(c)} & 0 & 0 & -\tilde{u}_{2,1}^{(e)} & -\tilde{u}_{2,2}^{(e)} \\ 1 & 0 & 0 & 0 & 0 & 0 & 0 & 0 & 1 & 0 \\ 0 & 1 & 1 & 0 & 0 & 0 & 0 & 0 & 0 & 1 \\ 0 & 0 & 0 & 1 & 1 & 0 & 0 & 0 & 0 & 0 \\ 0 & 0 & 0 & 0 & 0 & 0 & 1 & 1 & 0 & 1 \end{pmatrix}.$$

The first six rows are from matching conditions (7) and the rest are from the junctions rules (6). The array of initial conditions is given by

$$\tilde{\mathbf{b}} = \begin{pmatrix} (\tilde{u}_{1,1}^{(a)} - \tilde{u}_{2,2}^{(d)})c_1(0) + \tilde{u}_{1,2}^{(a)}c_2(0) - \tilde{u}_{2,1}^{(d)}c_4(0) \\ \tilde{u}_{2,1}^{(a)}c_1(0) + (\tilde{u}_{2,2}^{(a)} - \tilde{u}_{1,1}^{(b)})c_2(0) - \tilde{u}_{1,2}^{(b)}c_3(0) \\ \tilde{u}_{2,1}^{(a)}c_1(0) + (\tilde{u}_{2,2}^{(a)} - \tilde{u}_{1,1}^{(e)})c_2(0) - \tilde{u}_{1,2}^{(e)}c_4(0) \\ \tilde{u}_{2,1}^{(b)}c_2(0) + (\tilde{u}_{2,2}^{(b)} - \tilde{u}_{1,1}^{(c)})c_3(0) - \tilde{u}_{1,2}^{(c)}c_4(0) \\ -\tilde{u}_{1,2}^{(d)}c_1(0) + \tilde{u}_{2,1}^{(c)}c_3(0) + (\tilde{u}_{2,2}^{(c)} - \tilde{u}_{1,1}^{(d)})c_4(0) \\ -\tilde{u}_{2,1}^{(e)}c_2(0) + \tilde{u}_{2,1}^{(c)}c_3(0) + (\tilde{u}_{2,2}^{(c)} - \tilde{u}_{2,2}^{(e)})c_4(0) \\ 0 \\ 0 \\ 0 \\ 0 \end{pmatrix}.$$

Since the initial amplitude $c_i(0)$ distributed in different

subsystems for site i are the same, here label \mathcal{S} to indicate specific subsystem is neglected, and hence $c_i(0)$ needs to be substituted by the full amplitude $c_i(0)$ divided by corresponding connectivity n_i .

ACKNOWLEDGMENTS

This work is supported by Shanghai Sailing Program (16YF1412600); National Basic Research Program of China (2013CB922200); the National Natural Science Foundation of China (11420101003, 11604347, 91636105). T.-M. Yan thanks M. Weidemüller for remarks and suggestions.

-
- [1] E. Farhi and S. Gutmann, *Phys. Rev. A* **58**, 915 (1998).
- [2] A. M. Childs, *Phys. Rev. Lett.* **102**, 180501 (2009).
- [3] L. Valkunas, D. Abramavicius, and T. Mancal, *Molecular Excitation Dynamics and Relaxation: Quantum Theory and Spectroscopy*, 1st ed. (Wiley-VCH, Weinheim, 2013).
- [4] A. M. Childs and J. Goldstone, *Phys. Rev. A* **70**, 022314 (2004).
- [5] M. Mohseni, P. Rebentrost, S. Lloyd, and A. Aspuru-Guzik, *J. Chem. Phys.* **129**, 174106 (2008).
- [6] S. Bose, *Phys. Rev. Lett.* **91**, 207901 (2003).
- [7] O. Mülken and A. Blumen, *Phys. Rep.* **502**, 37 (2011).
- [8] R. Côté, A. Russell, E. E. Eyler, and P. L. Gould, *New J. Phys.* **8**, 156 (2006).
- [9] O. Mülken, A. Blumen, T. Amthor, C. Giese, M. Reetz-Lamour, and M. Weidemüller, *Phys. Rev. Lett.* **99**, 090601 (2007).
- [10] I. Foulger, S. Gnutzmann, and G. Tanner, *Phys. Rev. Lett.* **112**, 070504 (2014).
- [11] J. Böhm, M. Bellec, F. Mortessagne, U. Kuhl, S. Barkhofen, S. Gehler, H.-J. Stöckmann, I. Foulger, S. Gnutzmann, and G. Tanner, *Phys. Rev. Lett.* **114**, 110501 (2015).
- [12] H. B. Perets, Y. Lahini, F. Pozzi, M. Sorel, R. Morandotti, and Y. Silberberg, *Phys. Rev. Lett.* **100**, 170506 (2008).
- [13] A. Aspuru-Guzik and P. Walther, *Nat. Phys.* **8**, 285 (2012).
- [14] X. Qiang, T. Loke, A. Montanaro, K. Aungskunsiri, X. Zhou, J. L. O'Brien, J. B. Wang, and J. C. F. Matthews, *Nat. Comm.* **7**, 11511 (2016).
- [15] L. Novo, S. Chakraborty, M. Mohseni, H. Neven, and Y. Omar, *Sci. Rep.* **5**, 13304 (2015).
- [16] J. Janmark, D. A. Meyer, and T. G. Wong, *Phys. Rev. Lett.* **112**, 210502 (2014).
- [17] D. A. Meyer and T. G. Wong, *Phys. Rev. Lett.* **114**, 110503 (2015).
- [18] T. G. Wong, *Quant. Info. Proc.* **14**, 1767 (2015).
- [19] S. Salimi, *Quant. Info. Proc.* **9**, 75 (2010).
- [20] S.-i. Koda, *J. Chem. Phys.* **142**, 204112 (2015).
- [21] S. Sarkar, D. Kröber, and D. K. Morr, *Phys. Rev. Lett.* **117**, 226601 (2016).
- [22] R. v. Grondelle and V. I. Novoderezhkin, *Phys. Chem. Chem. Phys.* **8**, 793 (2006).
- [23] S. Yang, D. Z. Xu, Z. Song, and C. P. Sun, *J. Chem. Phys.* **132**, 234501 (2010).
- [24] G. D. Scholes, G. R. Fleming, A. Olaya-Castro, and R. van Grondelle, *Nat. Chem.* **3**, 763 (2011).